A State-similarity-based Fast Reliability Assessment for Power Systems with Variations of Generation and Load

Zeyu Liu, *Student Member IEEE*, Lewei Zhu, *Member, IEEE*, Kai Hou, *Senior Member, IEEE*, Yue Zhou, *Member, IEEE*, Ruifeng Zhao, *Member, IEEE*, Hongjie Jia, *Senior Member, IEEE*

***Abstract*—The increasing penetration of intermittent renewable generators and the uncertainty of loads have brought significant challenges to the power system reliability assessment, as large numbers of optimal power flow (OPF) tasks need to be repetitively solved considering these uncertainties. To deal with that, this paper proposes a state-similarity-based (SS) approach to replace the computationally demanding AC OPF. It is observed that the active constraints related to the least load curtailment typically remain consistent across varying system states. Following this, the active constraints are used to represent the state similarity, and then nonlinear equations are derived to replace the original AC OPF problems. Thereafter, an alternating iterative approach is developed to obtain the minimal load curtailment instead of calculating the time-consuming optimization. An optimality criterion is developed to exclude the majority of mismatched solutions, thereby minimizing potential inaccuracies in the reliability assessment. Case studies conducted on the RTS-79, IEEE 118-bus, and Brazilian systems demonstrate that the proposed methods can significantly enhance computational efficiency with minimal errors. In some instances, these methods can outperform traditional reliability assessment methods by over 10 times.**

***Index Terms*—State similarity, active constraints, reliability assessment, optimal power flow, renewable energy.**

I. Introduction

Electricity is universally acknowledged as a foundational pillar for national economic development and societal progression. A large-scale blackout would not only incur substantial societal impacts and immense economic losses, but could also threaten national security. In recent decades, the increasing penetration of renewable energy has brought more uncertainties and challenges to the security and stability of power system operations. Reliability assessment can quantify the system adequacy associated with these uncertainties, and therefore is indispensable for the planning and operation of power systems.

Generally, the reliability assessment comprises three processes [1]: system state selection, system state analysis, and reliability indices computation. In the first step, two fundamental methods [2]: Monte Carlo Simulation (MCS) and State Enumeration (SE) are used to select system states and calculate their respective probabilities. Next, the impact of each state (e.g., the minimal load curtailment) is obtained through optimal power flow (OPF). Finally, reliability indices are computed by multiplying the probability and impact of states. However, with the growing expansion of power systems and integration of fluctuating renewable energy, the analysis of a large number of states has resulted in an efficiency challenge for reliability assessment.

To deal with that, two main categories of approaches have been proposed. One is to reduce the number of systems states. Singh *et al*. [3] proposed a state-space pruning technique to reduce the number of samples, which can be implemented in Monte Carlo simulations. This is accomplished by removing coherent acceptance sets that have no loss of load states and performing proportional sampling over the other subspaces. In addition, several well-known variance reduction techniques have been employed to further accelerate the convergence of the MCS method [4], [5]. Compared with the MCS method, the SE method can reflect the relationship between system reliability and component reliability levels in a detailed manner [6]. However, it is prohibitive for SE to enumerate all possible system states and obtain accurate reliability indices. Therefore, most existing techniques reduce the number of system states in the SE method by only considering those states with significant contributions to reliability indices [7]. Jia *et al*. [8] proposed a fast contingency screening technique to search the most severe contingency states based on both probabilities and outage capacities. In our previous work [9], [10], Hou *et al*. proposed an impact-increment-based SE (IISE) approach to reduce the high-order contingency states implicitly. The partial contribution of higher-order contingencies can be transferred to the corresponding lower-order contingencies. While these approaches effectively reduce the number of system states, they present challenges in maintaining a balance between accuracy and efficiency, especially in power systems with high variations of renewable generation and load.

Another category of approaches is to accelerate OPF computations in the system state analysis. The AC OPF problem involves minimizing an objective function while subject to constraints. Since the 1960s, numerous optimization algorithms have been studied for efficient computations [11], [12]. However, these conventional model-based methods often encounter considerable computational challenges when repetitively analyzing a large number of states.

Recently, deep learning (DL) methods are increasingly

This work was supported in part by the National Natural Science Foundation of China (No. 52077150, U2066211, 52061635103) and in part by the National Key R&D Program of China (No. 2019YFE0118000). Paper no. TPWRS-01282-2023. (Corresponding author: Lewei Zhu.)

Z. Liu, K. Hou, and H. Jia are with the Key Laboratory of Smart Grid of Ministry of Education, and Tianjin Key Laboratory of Smart Energy and Information Technology, Tianjin University, Tianjin 300072, China. (e-mail: tjulzy@tju.edu.cn; khou@tju.edu.cn; hjjia@tju.edu.cn).

L. Zhu is with the Maritime College, Tianjin University of Technology, Tianjin 300384, China (e-mail: zhulewei@tju.edu.cn).

Y. Zhou is with the School of Engineering, Cardiff University, Cardiff CF24 3AA, U.K. (email: zhouy68@cardiff.ac.uk).

R. Zhao is with the Electric Power Dispatching and Control Center, Guangdong Power Grid Company Ltd., Guangzhou 510600, China. (email: ruifzhao@126.com).

recognized as a promising data-driven approach for OPF problems, providing an alternative to conventional optimization algorithms. These DL-based methods utilize neural networks to establish a model-free, end-to-end mapping, effectively transferring OPF computations to the offline training phase [13], [14]. Existing studies show that well-trained neural networks can deliver solutions with high precision, achieving speeds 100 to 1000 times faster than traditional model-driven approaches. However, these superior performances have been validated only on specific test sets, lacking guaranteed accuracy for scenarios not covered in these sets. This limitation is particularly critical in safety-sensitive applications, like reliability assessments [15]. Consequently, the black-box nature of data-driven methods restricts their verifiability and trustworthiness, limiting their practical applicability in power systems. Moreover, intensive data preparation and generalizability also present challenges [16]. For each system case, it is necessary to generate new training data through simulations using model-based approaches. Generally, the volume of such training data is considerably larger than that needed for traditional reliability assessments, inevitably leading to a greater computational burden in the offline phase.

For numerous OPF computations in reliability assessment, further advancement in model-based methods remains crucial. Recognizing that OPF problems exhibit only minor variations with changes in generators or loads, a novel approach is being explored. This strategy aims to derive new solutions directly from those of similar OPF problems. Safdarian *et al*. [17] used the post optimal analysis to determine the solution by imposing differences concerning the base case, instead of optimizing all DC OPF problems independently. Yong *et al*. [18], [19] proposed a multi-parametric-linear-programming-based method to reduce the calculations of DC OPF problems. The load variations are treated as MPLP parameters and massive system states can be analyzed efficiently by matching with their identical optimal basis. Deka *et al.* [20] utilized DNN to classify states based on their similarities, identifying the relationship between uncertain injection data and active constraint sets. Our previous work [21], [22] constructed a Lagrange-multipliers-based linear function to derive the relationship between the minimal load curtailment and the variations of system states. However, due to the nonlinearity of the AC OPF model, these methods are not applicable.

To deal with these issues, our study aims at exploiting the similarities among AC OPF problems to accelerate system state analysis. Typically, the minimal load curtailment serves as the optimization objective of AC OPF in reliability assessment. Interestingly, empirical evidence suggests that these load curtailments are usually induced by certain violated or active constraints. Moreover, these constraints often remain active despite changes in AC OPF parameters. Consequently, these consistently active constraints can be used to characterize the state similarity across various AC OPF problems. To this end, we propose a state-similarity-based approach (SS) that replaces the AC OPF with a system of nonlinear equations. This approach allows us to obtain the optimal load curtailment by solving a set of nonlinear equations rather than solving optimization problems, significantly enhancing the computational efficiency of reliability assessment. The main contributions are as follows:

1) The active constraints are used as the state similarity to construct a system of nonlinear equations, and the state-similarity-based approach is proposed to obtain the optimal solutions by solving equations, instead of cumbersome AC OPF optimizations.

2) An alternating iterative approach is developed to derive solutions from the underdetermined system of nonlinear equations. Additionally, optimality criteria are carried out to guarantee the accuracy of reliability assessment.

3) The proposed SS approach can be integrated with existing state reduction techniques, such as the impact-increment and cross-entropy methods, to further enhance the efficiency of reliability assessment methods.

The rest of the paper is organized as follows: Section II introduces the problem statement and solution framework. The proposed SS approach is described in Section III. Case studies are performed in Section IV and conclusions are drawn in Section V.

II. Problem Statement and Solution Framework

A. Reliability Assessment of Power Systems

Reliability assessment involves analyzing the impact of selected system states and providing quantified reliability indices. In this study, the framework of the proposed method is presented in Fig. 1 and explained as follows,

1) *System State Selection*. Use either MCS or SE to create the system state set Ω_s. The number of sampled system states N_{MCS} and the maximum contingency order N_{T} serve as the stopping criteria, respectively.

Most power system contingencies can be represented by the system states in Ω_s. Each system state $\boldsymbol{s}$ can be characterized by a vector as follows,

$$\boldsymbol{s}=\begin{bmatrix}\boldsymbol{s}_l & \boldsymbol{s}_g & \boldsymbol{S}_d & \boldsymbol{S}_{g\min} & \boldsymbol{S}_{g\max}\end{bmatrix} \tag{1}$$

where $\boldsymbol{s}_l$ is the n_l×1 vector of the status indicators of transmission lines; $\boldsymbol{s}_g$ is the n_g×1 vector of the status indicators of generators; $\boldsymbol{S}_d$ is the n_b×1 vector of bus loads; $\boldsymbol{S}_{g\min}$ and $\boldsymbol{S}_{g\max}$ are the n_g×1 vectors of the minimal and maximal outputs of generators; n_b, n_g, and n_l are the numbers of buses, generators, and branches. Both conventional generators (CG) and renewable energy generators (REG) are incorporated in power systems, and the output values of the REGs are derived from their annual output curves. n_t denotes the number of time periods for the load and the REG values, considering their time-dependent correlation.

2) *System State Analysis*. The system state analysis is based on the OPF solutions, which assess whether load curtailment is required to maintain the system within operational constraints during contingencies, load variations, and REG fluctuations.

The objective of AC OPF is to minimize the total load curtailment. This is formulated as follows,

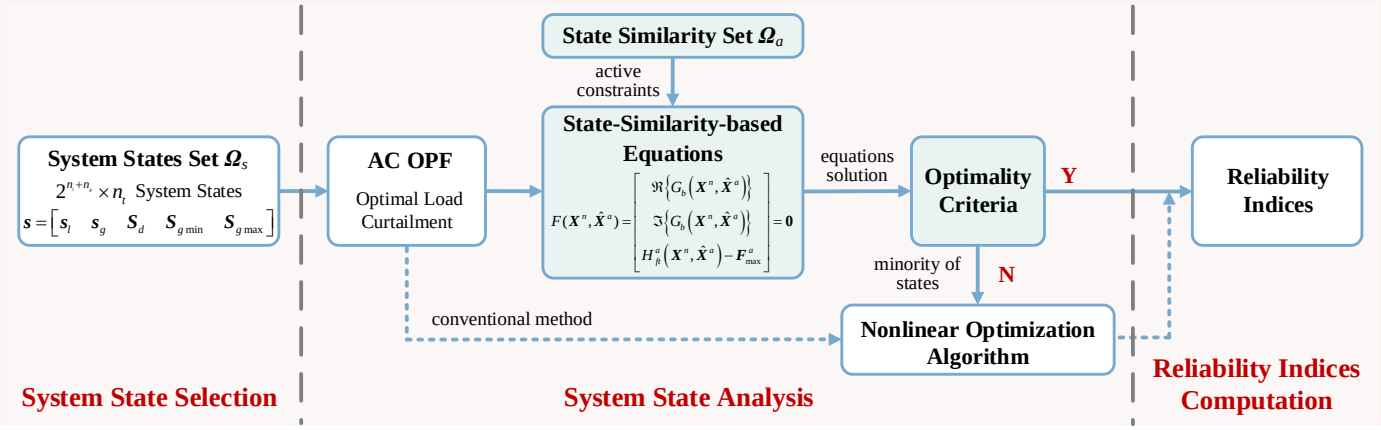

Fig. 1. The framework of the proposed reliability assessment method.

$$\min \quad f_{LC}=\sum \boldsymbol{P}_{LC} \tag{2}$$

Subject to

$$G_b(\boldsymbol{V},\boldsymbol{S}_g,\boldsymbol{S}_{LC})=[\boldsymbol{V}]\boldsymbol{Y}_{bus}\boldsymbol{V}^*-\boldsymbol{C}_g\boldsymbol{S}_g-\boldsymbol{S}_{LC}+\boldsymbol{S}_d=0 \tag{3}$$

$$\left|\boldsymbol{Y}_{ft}\boldsymbol{V}\right|\le \boldsymbol{F}_{\max} \tag{4}$$

$$\boldsymbol{U}_{\min}\le \boldsymbol{U}\le \boldsymbol{U}_{\max} \tag{5}$$

$$\boldsymbol{\theta}_{\min}\le \boldsymbol{\theta}\le \boldsymbol{\theta}_{\max} \tag{6}$$

$$\boldsymbol{P}_{g\min}\le \boldsymbol{P}_g\le \boldsymbol{P}_{g\max} \tag{7}$$

$$\boldsymbol{Q}_{g\min}\le \boldsymbol{Q}_g\le \boldsymbol{Q}_{g\max} \tag{8}$$

$$\boldsymbol{0}\le \boldsymbol{P}_{LC}\le \boldsymbol{P}_d \tag{9}$$

$$\boldsymbol{0}\le \boldsymbol{Q}_{LC}\le \boldsymbol{Q}_d \tag{10}$$

where f_{LC} is the objective function; $\boldsymbol{S}_{LC}$ is the $n_b\times 1$ vector of the complex load curtailment, $\boldsymbol{S}_{LC}=\boldsymbol{P}_{LC}+j\boldsymbol{Q}_{LC}$; G_b represents the bus power flow balance constraints; $\boldsymbol{V}$ is the $n_b\times 1$ vector of the complex bus voltage, $\boldsymbol{U}$ and $\boldsymbol{\theta}$ are the $n_b\times 1$ vectors of the bus voltage magnitudes and angles, $\boldsymbol{V}=\boldsymbol{U}e^{j\boldsymbol{\theta}}$; $\boldsymbol{S}_d$ is the $n_b\times 1$ vector of the complex power load, $\boldsymbol{S}_d=\boldsymbol{P}_d+j\boldsymbol{Q}_d$; $\boldsymbol{S}_g$ is the $n_g\times 1$ vector of the generator complex power output, $\boldsymbol{S}_g=\boldsymbol{P}_g+j\boldsymbol{Q}_g$; $\boldsymbol{Y}_{bus}$ is the bus admittance matrix; $\boldsymbol{C}_g$ is the generator connection matrix; (4) represents the branch flow limits; $\boldsymbol{Y}_{ft}$ is the branch admittance matrix; (5) and (6) represent the voltage magnitude and angle limits; (7) and (8) represent the generator real and reactive output limits, $\boldsymbol{S}_{g\min}=\boldsymbol{P}_{g\min}+j\boldsymbol{Q}_{g\min}$, $\boldsymbol{S}_{g\max}=\boldsymbol{P}_{g\max}+j\boldsymbol{Q}_{g\max}$.

3) *Reliability Indices Computation*. The general formula for calculating reliability indices is,

$$R=\sum_{\boldsymbol{s}\in\Omega_s} P(\boldsymbol{s})I(\boldsymbol{s}) \tag{11}$$

where R is the reliability index; $P(\boldsymbol{s})$ is the probability of state $\boldsymbol{s}$; $I(\boldsymbol{s})$ represents the consequence of state $\boldsymbol{s}$. Different forms of $I(\boldsymbol{s})$ correspond to various reliability indices.

In this study, the expected energy not supplied (EENS) and probability of load curtailments (PLC) are used as reliability indices,

$$EENS=T\sum_{\boldsymbol{s}\in\Omega_s} P(\boldsymbol{s})I(\boldsymbol{s}) \tag{12}$$

$$PLC=\sum_{\boldsymbol{s}\in\Omega_s} P(\boldsymbol{s})I_{LCF}(\boldsymbol{s}) \tag{13}$$

$$I_{LCF}(\boldsymbol{s})=\begin{cases}1, & I_{LC}(\boldsymbol{s})>0\\ 0, & I_{LC}(\boldsymbol{s})=0\end{cases} \tag{14}$$

where $I_{LC}(\boldsymbol{s})$ and $I_{LCF}(\boldsymbol{s})$ are the load curtailment and load curtailment indicator of state $\boldsymbol{s}$, respectively; T is the evaluated time, typically one year.

B. Challenges and Proposed Solution Framework

During Step 2, the most significant challenge for reliability assessment is evaluating numerous system states, because it requires repeatedly solving AC OPF problems with optimization algorithms.

Generally, for reliability assessment, load curtailments of AC OPF problems primarily are driven by binding or active constraints, such as transmission and generation capacity limits. Furthermore, the minimal load curtailments of AC OPF problems corresponding to various states often share the same active constraints. Consequently, ***state similarity*** is defined as a condition in which different AC OPF problems exhibit identical sets of active constraints at their optimal solutions. These active constraints thus represent indicators of state similarity across diverse system states.

As illustrated in Fig. 1, the proposed state similarity approach is used as an alternative way to the complex optimizations involved in AC OPF. This method is highly effective when a new state is similar to a previously analyzed one, i.e., they share the same active constraints for AC OPF.

A fundamental component of this approach is the establishment of a state similarity set, denoted as Ω_a. This set acts as a repository that collects active constraint sets identified during the reliability assessment. Each active constraint set in Ω_a represents a specific category of similar states. When evaluating a new state, a crucial step involves searching through Ω_a to find a set of active constraints that potentially align with the new state. It begins by sequentially applying each active constraint set from Ω_a to formulate the state-similarity-based equations. The solutions derived from these equations are then verified through optimality criteria. This matching process continues until a solution satisfying the optimality criteria is found or all active constraint sets in Ω_a

have been exhaustively tested. If the criteria are satisfied, it indicates that the new state is similar to a previously analyzed state. This allows for the calculation of optimal load curtailment based on the obtained solution. Conversely, if none of the active constraint sets in Ω_a are applicable, it implies that the new state is unique and does not share similarities with any previously analyzed states. In such cases, OPF optimization algorithms are employed to determine the optimal load curtailment for these unmatched states. The active constraint set derived from the AC OPF optimization results is then added to Ω_a, contributing a new pattern of state similarity.

Due to slight variations in generators, loads, or REGs among the AC OPF problems of numerous states, only a few sets of active constraints exist in Ω_a for the entire reliability assessment. The majority of system states are evaluated by the state-similarity-based equations, while the minority of states will be analyzed by the nonlinear optimization algorithms. In this way, the proposed approach can dramatically improve the computational efficiency of the reliability assessment.

The framework of the proposed state-similarity-based reliability assessment method involves three key steps, which are explained in Section III.

1) Transform AC OPF into a system of equations;
2) Obtain a solution to the equations;
3) Develop optimality criteria for the obtained solutions.

III. Proposed State Similarity-Based Approach

A. State Similarity in the AC OPF Model

In the reliability assessment, the AC OPF with the minimum load curtailment (2) - (10) is a nonlinear programming (NLP) problem [23], which can be described in a general form,

$$\begin{aligned} &\min \quad f(\boldsymbol{X}) \\ s.t. \quad &G(\boldsymbol{X}) = \begin{bmatrix} \Re\{G_b(\boldsymbol{X})\} \\ \Im\{G_b(\boldsymbol{X})\} \end{bmatrix}_{2n_b\times 1} = \boldsymbol{0} \\ &H(\boldsymbol{X}) = \begin{bmatrix} H_{ft}(\boldsymbol{X}) - \boldsymbol{F}_{\max} \\ \boldsymbol{A}_I \boldsymbol{X} - \boldsymbol{B}_I \end{bmatrix}_{(2n_l+8n_b+4n_g)\times 1} \le \boldsymbol{0} \end{aligned} \tag{15}$$

$$\boldsymbol{X} = \begin{bmatrix} \boldsymbol{\theta} & \boldsymbol{U} & \boldsymbol{P}_g & \boldsymbol{Q}_g & \boldsymbol{P}_{LC} & \boldsymbol{Q}_{LC} \end{bmatrix}^T \tag{16}$$

where f is the objective function; G and H are the equality and inequality constraints, respectively; $\boldsymbol{X}$ is the variables; $\Re$ and $\Im$ represent the real and imaginary parts; $H_{ft}(\boldsymbol{X})$ represents the branch complex power flow in (4); $\boldsymbol{A}_I$ and $\boldsymbol{B}_I$ represent the coefficient matrices of the variables limits in (5) - (10).

In the AC OPF problem (15) - (16), an *active constraint* is a constraint that is tightly bound or exactly satisfied at the optimal solution point. Equality constraints are invariably active, as they must be exactly satisfied in any feasible solution. On the other hand, an inequality constraint is considered active at the optimal solution when it is satisfied as an equality. This means that the solution is precisely on the boundary defined by that constraint. Consequently, the set of *active constraints* $\mathcal{A}$ consists of all equality constraints and those inequality constraints that are binding at the optimal solution,

$$\mathcal{A} = \{G\} \bigcup \left\{ H_i \middle| H_i(\boldsymbol{X}^*) = 0 \right\} \tag{17}$$

where $\boldsymbol{X}^*$ is the optimal solution; H_i represents the ith inequality constraint, and each inequality constraint must be either: (a) *active*: $H_i(\boldsymbol{X}^*) = 0$, or (b) *inactive*: $H_i(\boldsymbol{X}^*) < 0$. In terms of the AC OPF problem, it has been demonstrated that the active constraints are relatively insensitive to variations in loads and REGs [24]. Moreover, most inequality constraints are inactive in numerous cases [25]. Therefore, various AC OPF problems usually exhibit state similarity, regardless of the differences in loads and REG outputs.

For example, state similarity is observed between the two states in a 3-bus system, as shown in Fig. 2. Bus 1 is the slack bus with an angle of 0, G2 is a REG, and the impedance of all three lines is 0.02 + j0.06 (p.u.). The loads and generation capabilities of the two states are given in Table 1.

TABLE I
THREE-BUS SYSTEM STATES

State	Load (MW + jMvar)			Generation Capability (MW + jMvar)	
	1	2	3	G1	G2
S1	100 + j50	100 + j50	100 + j50	200 ± j100	90 ± j100
S2	90 + j45	50 + j25	90 + j45	200 ± j100	45 ± j50

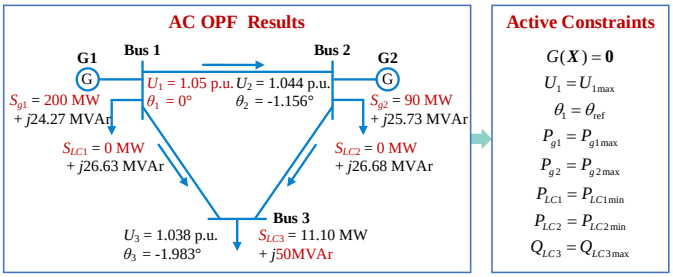

(a) AC OPF problem for S1.

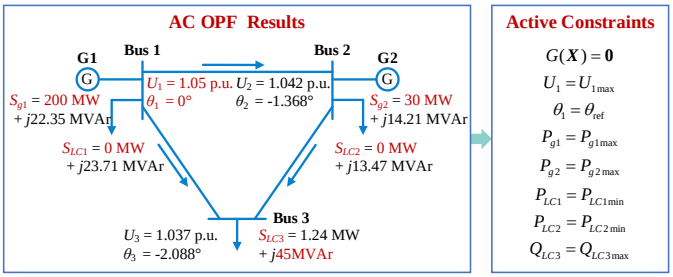

(b) AC OPF problem for S2.

Fig. 2. An example of state similarity for two states in the 3-bus system.

As illustrated in Fig. 2, states S1 and S2 demonstrate state similarity because they activate identical constraints, indicating that these constraints have reached their respective limits,

$$\mathcal{A} = \begin{Bmatrix} \Re\{G_b(\boldsymbol{X})\} = 0 \\ \Im\{G_b(\boldsymbol{X})\} = 0 \end{Bmatrix} \bigcup \begin{Bmatrix} U_1 = U_{1\max} & P_{LC1} = P_{LC1\min} \\ \theta_1 = 0 & P_{LC2} = P_{LC2\min} \\ P_{g1} = P_{g1\max} & Q_{LC3} = Q_{LC3\max} \\ P_{g2} = P_{g2\max} & \end{Bmatrix} \tag{18}$$

It should be noted that the same active constraints do not necessarily mean that identical limit values are reached. For example, despite the differing output values of P_{g2} in the two states, P_{g2} reaches its maximum output in both states. This

indicates the activation of identical constraints. The variation in constraint values denotes the distinction between states, while the activation of identical constraints underscores their underlying similarity. In the 3-bus system, this similarity implies that both generators, G1 and G2, are operating at their maximum active power output. Simultaneously, the voltage at Bus 1 is sustained at its upper limit, and the load curtailment constraints are active.

Variables subjected to these active constraints are referred to as *active variables*, denoted as $\boldsymbol{X}^a$. As active variables having predetermined values, they can be treated as known constants within the variable vector $\boldsymbol{X}$. Then, the other variables that do not reach their respective limits are termed as *non-active variables*, denoted as $\boldsymbol{X}^n$.

Upon substituting (18) into the AC OPF problem, we obtain a system of equations,

$$F(\boldsymbol{X}, \boldsymbol{X}^a = \hat{\boldsymbol{X}}^a) = F(\boldsymbol{X}^n, \hat{\boldsymbol{X}}^a) = \begin{bmatrix} \Re\left\{G_b\left(\boldsymbol{X}^n, \hat{\boldsymbol{X}}^a\right)\right\} \\ \Im\left\{G_b\left(\boldsymbol{X}^n, \hat{\boldsymbol{X}}^a\right)\right\} \end{bmatrix} = \boldsymbol{0} \tag{19}$$

$$\boldsymbol{X}^n = \begin{bmatrix} U_2 & U_3 & \theta_2 & \theta_3 & Q_{g1} & Q_{g2} & P_{LC3} & Q_{LC1} & Q_{LC2} \end{bmatrix} \tag{20}$$

$$\boldsymbol{X}^a = \begin{bmatrix} U_1 & \theta_1 & P_{g1} & P_{g2} & P_{LC1} & P_{LC2} & Q_{LC3} \end{bmatrix} \tag{21}$$

$$\hat{\boldsymbol{X}}^a = \begin{bmatrix} U_{1\max} & 0 & P_{g1\max} & P_{g2\max} & P_{LC1\min} & P_{LC2\min} & Q_{LC3\max} \end{bmatrix} \tag{22}$$

where $\hat{\boldsymbol{X}}^a$ represents the values of active variables $\boldsymbol{X}^a$.

The active constraints of one state are determined by optimizing the solution to the AC OPF problem. Subsequently, these identified active constraints enable the transformation of the AC OPF for a different state into a system of equations.

Based on the general form of AC OPF problem (15) - (16), the state-similarity-based equations $F(\boldsymbol{X}^n, \hat{\boldsymbol{X}}^a)$ can be represented as follows,

$$F(\boldsymbol{X}^n, \hat{\boldsymbol{X}}^a) = \begin{bmatrix} \Re\left\{G_b\left(\boldsymbol{X}^n, \hat{\boldsymbol{X}}^a\right)\right\} \\ \Im\left\{G_b\left(\boldsymbol{X}^n, \hat{\boldsymbol{X}}^a\right)\right\} \\ H_{ft}^a\left(\boldsymbol{X}^n, \hat{\boldsymbol{X}}^a\right) - \boldsymbol{F}_{\max}^a \end{bmatrix}_{(2n_b + a_l) \times (4n_b + 2n_g - a_x)} = \boldsymbol{0} \tag{23}$$

$$\boldsymbol{X}^n = \begin{bmatrix} \boldsymbol{\theta}^n & \boldsymbol{U}^n & \boldsymbol{P}_g^n & \boldsymbol{Q}_g^n & \boldsymbol{P}_{LC}^n & \boldsymbol{Q}_{LC}^n \end{bmatrix}^T \tag{24}$$

$$\boldsymbol{X}^a = \hat{\boldsymbol{X}}^a = \begin{bmatrix} \hat{\boldsymbol{\theta}}^a & \hat{\boldsymbol{U}}^a & \hat{\boldsymbol{P}}_g^a & \hat{\boldsymbol{Q}}_g^a & \hat{\boldsymbol{P}}_{LC}^a & \hat{\boldsymbol{Q}}_{LC}^a \end{bmatrix}^T \tag{25}$$

where $H_{ft}^a(\boldsymbol{X}^n, \hat{\boldsymbol{X}}^a) - \boldsymbol{F}_{\max}^a$ represents the active constraints of branch power flow; a_l and a_x represent the number of active branch constraints and active variables, respectively.

If the active constraints match the states, then the optimal solution to AC OPF is the solution to equations (23) - (25). Nevertheless, since the number of variables ($4n_b + 2n_g - a_x$) is significantly greater than ($2n_b + a_l$), the system of equations has an infinite number of solutions. To address this, Section III.B proposes an alternating iterative approach aimed at finding a solution that closely approximates the optimal solution to AC OPF. Furthermore, acknowledging that the obtained solution may not always be the optimal solution to AC OPF due to the disregarded inequality constraints or mismatched active constraints, an optimality criterion is developed in Section III.C. to filter out the incorrect solutions. As a result, it can accelerate the analysis of numerous similar states, eliminating the need to solve each similar AC OPF problem independently.

B. Proposed Alternating Iterative Approach to Solving Equations

The Newton method is one of the most popular approaches to approximate solutions to nonlinear systems when the number of unknowns equals the number of equations. Considering a system of nonlinear equations $F(\boldsymbol{X}) = \boldsymbol{0}$, we can calculate the solution $\boldsymbol{X}$,

$$\Delta \boldsymbol{X}^{(i)} = -\left[\boldsymbol{J}(\boldsymbol{X}^{(i)})\right]^{-1} F(\boldsymbol{X}^{(i)}) \tag{26}$$

$$\boldsymbol{X}^{(i+1)} = \boldsymbol{X}^{(i)} + \Delta \boldsymbol{X}^{(i)} \tag{27}$$

where i is the iteration counter; $\boldsymbol{J}$ is the Jacobi matrix.

Given the underdetermined nature of the state-similarity-based equations (23) - (25), resulting in $\Delta \boldsymbol{X}^{(i)}$ possessing infinite solutions, we propose an alternating iterative approach. This method involves dividing the system of equations (23) into two parts,

$$F(\boldsymbol{X}_\alpha^n, \boldsymbol{X}_\beta^n, \hat{\boldsymbol{X}}^a) = \left[\begin{array}{c|c} \Re\{[\boldsymbol{V}]\boldsymbol{Y}_{bus}\boldsymbol{V}^* - \boldsymbol{G}_\beta\} & \Re\{\boldsymbol{G}_\alpha - \boldsymbol{S}_b + \boldsymbol{S}_d\} \\ \Im\{[\boldsymbol{V}]\boldsymbol{Y}_{bus}\boldsymbol{V}^* - \boldsymbol{G}_\beta\} & \Im\{\boldsymbol{G}_\alpha - \boldsymbol{S}_b + \boldsymbol{S}_d\} \\ H_{ft}^a\left(\boldsymbol{X}_\alpha^n, \hat{\boldsymbol{X}}_\alpha^a\right) - \boldsymbol{F}_{\max}^a & \end{array}\right] = \boldsymbol{0} \tag{28}$$

where $\boldsymbol{G}_\alpha$ and $\boldsymbol{G}_\beta$ denote the respective parts of the $G_b(\boldsymbol{X}^n)$.

The first part is a system of nonlinear equations F_α,

$$F_\alpha(\boldsymbol{X}_\alpha^n, \boldsymbol{X}_\beta^n, \hat{\boldsymbol{X}}_\alpha^a) = \begin{bmatrix} \Re\{[\boldsymbol{V}]\boldsymbol{Y}_{bus}\boldsymbol{V}^* - \boldsymbol{G}_\beta\} \\ \Im\{[\boldsymbol{V}]\boldsymbol{Y}_{bus}\boldsymbol{V}^* - \boldsymbol{G}_\beta\} \\ H_{ft}^a\left(\boldsymbol{X}_\alpha^n, \hat{\boldsymbol{X}}_\alpha^a\right) - \boldsymbol{F}_{\max}^a \end{bmatrix}_{(2n_b + a_l) \times (2n_b - a_\alpha)} = \boldsymbol{0} \tag{29}$$

$$\boldsymbol{X}_\alpha^n = \begin{bmatrix} \boldsymbol{\theta}^n & \boldsymbol{U}^n \end{bmatrix}^T \tag{30}$$

$$\hat{\boldsymbol{X}}_\alpha^a = \begin{bmatrix} \hat{\boldsymbol{\theta}}^a & \hat{\boldsymbol{U}}^a \end{bmatrix}^T \tag{31}$$

where $\boldsymbol{V} = \boldsymbol{U}e^{j\boldsymbol{\theta}}$; $\boldsymbol{U}$ and $\boldsymbol{\theta}$ are each divided into non-active ($\boldsymbol{U}^n, \boldsymbol{\theta}^n$) and active ($\hat{\boldsymbol{U}}^a, \hat{\boldsymbol{\theta}}^a$) components; a_α represents the number of active variables.

Another part is a system of linear equations F_β,

$$F_\beta(\boldsymbol{X}_\alpha^n, \boldsymbol{X}_\beta^n, \hat{\boldsymbol{X}}_\beta^a) = \begin{bmatrix} \Re\{\boldsymbol{G}_\alpha - \boldsymbol{S}_b + \boldsymbol{S}_d\} \\ \Im\{\boldsymbol{G}_\alpha - \boldsymbol{S}_b + \boldsymbol{S}_d\} \end{bmatrix}_{(2n_b - a_\beta) \times (2n_b - a_\beta)} = \boldsymbol{0} \tag{32}$$

$$\boldsymbol{X}_\beta^n = \begin{bmatrix} \boldsymbol{P}_b^n & \boldsymbol{Q}_b^n \end{bmatrix}^T \tag{33}$$

$$\hat{\boldsymbol{X}}_\beta^a = \begin{bmatrix} \hat{\boldsymbol{P}}_b^a & \hat{\boldsymbol{Q}}_b^a \end{bmatrix}^T \tag{34}$$

where $\boldsymbol{S}_b = \boldsymbol{P}_b + j\boldsymbol{Q}_b = \boldsymbol{C}_g\boldsymbol{S}_g + \boldsymbol{S}_{LC}$ is the vector of bus power injection; $\boldsymbol{P}_b$ and $\boldsymbol{Q}_b$, comprising both non-active and active components, represent the real and reactive bus power injections, respectively; a_β represents the number of active variables in them.

Then, we update the two unknowns $\boldsymbol{X}_\alpha^n$ and $\boldsymbol{X}_\beta^n$ iteratively,

$$\Delta \boldsymbol{X}_{\alpha}^{n(i)} = -\left(\boldsymbol{J}_{\alpha}^{(i)}\right)^{-1} F_{\alpha}(\boldsymbol{X}_{\alpha}^{n(i)}, \boldsymbol{X}_{\beta}^{n(i+1)}, \hat{\boldsymbol{X}}_{\alpha}^{a}) \tag{35}$$

$$\boldsymbol{X}_{\alpha}^{n(i+1)} = \boldsymbol{X}_{\alpha}^{n(i)} + \Delta \boldsymbol{X}_{\alpha}^{n(i)} \tag{36}$$

where $\boldsymbol{J}_{\alpha}^{(i)}$ is denoted by

$$\boldsymbol{J}_{\alpha}^{(i)} = \begin{bmatrix} \Re\{G_{b,\theta}(\boldsymbol{X}_{\alpha}^{n(i)}, \boldsymbol{X}_{\beta}^{n(i+1)}, \hat{\boldsymbol{X}}_{\alpha}^{a})\} & \Re\{G_{b,U}^{s}(\boldsymbol{X}_{\alpha}^{n(i)}, \boldsymbol{X}_{\beta}^{n(i+1)}, \hat{\boldsymbol{X}}_{\alpha}^{a})\} \\ \Im\{G_{b,\theta}(\boldsymbol{X}_{\alpha}^{n(i)}, \boldsymbol{X}_{\beta}^{n(i+1)}, \hat{\boldsymbol{X}}_{\alpha}^{a})\} & \Im\{G_{b,U}^{s}(\boldsymbol{X}_{\alpha}^{n(i)}, \boldsymbol{X}_{\beta}^{n(i+1)}, \hat{\boldsymbol{X}}_{\alpha}^{a})\} \\ H_{ft,\theta}^{a}(\boldsymbol{X}_{\alpha}^{n(i)}, \hat{\boldsymbol{X}}_{\alpha}^{a}) & H_{ft,U}^{a}(\boldsymbol{X}_{\alpha}^{n(i)}, \hat{\boldsymbol{X}}_{\alpha}^{a}) \end{bmatrix} \tag{37}$$

Since (35) is an overdetermined system with more equations than unknowns, the least squares approach is utilized to find an approximate solution for $\Delta \boldsymbol{X}_{\alpha}^{n(i)}$ [26].

Similarly,

$$\Delta \boldsymbol{X}_{\beta}^{n(i)} = -\left(\boldsymbol{J}_{\beta}^{(i)}\right)^{-1} F_{\beta}(\boldsymbol{X}_{\alpha}^{n(i)}, \boldsymbol{X}_{\beta}^{n(i)}, \hat{\boldsymbol{X}}_{\beta}^{a}) \tag{38}$$

$$\boldsymbol{X}_{\beta}^{n(i+1)} = \boldsymbol{X}_{\beta}^{n(i)} + \Delta \boldsymbol{X}_{\beta}^{n(i)} \tag{39}$$

where $\boldsymbol{J}_{\beta}^{(i)}$ is denoted by

$$\boldsymbol{J}_{\beta}^{(i)} = -\boldsymbol{I}_{(2n_b - a_\beta)\times(2n_b - a_\beta)} \tag{40}$$

It is clear that (38) is a system of linear equations with an equal number of equations and unknowns, allowing us to directly obtain a unique solution for $\Delta \boldsymbol{X}_{\beta}^{n(i)}$.

Equations (35) - (37) and (38) - (40) are alternated iteratively until either the maximum number of iterations $N_{\max}$ is reached, or the acceptable tolerance *tol* is achieved,

$$i > N_{\max} \tag{41}$$

$$\left\| F(\boldsymbol{X}_{\alpha}^{n(i)}, \boldsymbol{X}_{\beta}^{n(i)}, \hat{\boldsymbol{X}}^{a}) \right\|_{\infty} < tol \tag{42}$$

Following this iterative process, the derived solution is then evaluated against the feasibility criterion,

$$H(\boldsymbol{X}_{\alpha}^{n(i)}, \boldsymbol{X}_{\beta}^{n(i)}, \hat{\boldsymbol{X}}^{a}) \le 0 \tag{43}$$

If the solution is feasible, we obtain a solution to the state-similarity-based equations (23) - (25). If not, the solution process is considered failed, indicating that the selected active constraints are not suitable for this state.

C. Optimality Criteria of Solutions

The optimality criteria are developed to check the optimality of the obtained solution $\boldsymbol{X}^{s}$. If it fails, the erroneous solution is filtered out to improve computational precision.

If the load curtailment of the obtained solution $\boldsymbol{X}^{s}$ equals zero, then $\boldsymbol{X}^{s}$ is an optimal solution. When the load curtailment is non-zero, the *Kraush-Kuhn-Tucker* (KKT) condition is used to judge whether the feasible solution $\boldsymbol{X}^{s}$ is an optimal solution. If $\boldsymbol{X}^{s}$ is the optimal solution $\boldsymbol{X}^{*}$, then there exists $\boldsymbol{\lambda}^{*} = \left(\lambda_1^{*}, \ldots, \lambda_{2n_b}^{*}\right)$ and $\boldsymbol{\mu}^{*} = \left(\mu_1^{*}, \ldots, \mu_{(a_l + a_x)}^{*}\right)$ such that

$$\nabla f\left(\boldsymbol{X}^{*}\right) + \sum_{j=1}^{2n_b} \lambda_j^{*} \nabla G_j\left(\boldsymbol{X}^{*}\right) + \sum_{k=1}^{a_l + a_x} \boldsymbol{\mu}_k^{*} \nabla H_k\left(\boldsymbol{X}^{*}\right) = 0 \tag{44}$$

$$\boldsymbol{\mu}_k^{*} \ge 0 \quad k = 1, 2, \ldots, (a_l + a_x) \tag{45}$$

Theorem 1 [27]: Consider the system $\boldsymbol{A}_{m\times n}\boldsymbol{x}_{n\times 1} = \boldsymbol{b}_{n\times 1}$, with coefficient $\boldsymbol{A}$ and augmented matrix $[\boldsymbol{A}|\boldsymbol{b}]$. The possibilities for solving the system are

(i) $\boldsymbol{Ax} = \boldsymbol{b}$ is inconsistent (i.e., no solution exists) if and only if rank[$\boldsymbol{A}$] < rank[$\boldsymbol{A}|\boldsymbol{b}$].

(ii) $\boldsymbol{Ax} = \boldsymbol{b}$ has a unique solution if and only if rank[$\boldsymbol{A}$] = rank[$\boldsymbol{A}|\boldsymbol{b}$] = n.

(iii) $\boldsymbol{Ax} = \boldsymbol{b}$ has infinitely many solutions if and only if rank[$\boldsymbol{A}$] = rank[$\boldsymbol{A}|\boldsymbol{b}$] < n.

Considering the determination of the specific values of $\boldsymbol{\lambda}^{*}$ and $\boldsymbol{\mu}^{*}$ is not required, and that merely confirming the existence of a solution is sufficient, we employ the following condition to determine whether it satisfies the optimality criteria (44) and (45),

$$\begin{aligned} &rank\left[\sum \boldsymbol{\lambda}^{*} \nabla G\left(\boldsymbol{X}^{*}\right) + \sum \boldsymbol{\mu}^{*} \nabla H\left(\boldsymbol{X}^{*}\right)\right] = \\ &rank\left[\sum \boldsymbol{\lambda}^{*} \nabla G\left(\boldsymbol{X}^{*}\right) + \sum \boldsymbol{\mu}^{*} \nabla H\left(\boldsymbol{X}^{*}\right) \middle| -\nabla f\left(\boldsymbol{X}^{*}\right)\right] \end{aligned} \tag{46}$$

The AC OPF problem is inherently non-convex due to its nonlinear power flow equations and various operational constraints. This non-convexity implies that the KKT conditions are necessary but not sufficient for determining optimality in AC OPF problems. Therefore, a solution that satisfies the KKT conditions may only represent a local optimum rather than a global one [28]. Currently, no universally applicable method can consistently guarantee finding the global optimum in all scenarios. A large number of KKT-based methods have been widely employed to solve AC OPF problems, though they may yield locally optimal solutions [29], [30]. In practical applications, the solution provided by optimization solvers often exhibits a negligible gap from the optimum. As a result, these solutions are usually accepted as global solutions, despite the inherent limitations of the KKT conditions.

In this study, the active constraints are derived from the globally optimal solutions of the base states, which are obtained through optimization solvers. Therefore, a feasible solution that satisfies the same active constraints and the KKT condition is highly likely to be an optimal solution. Moreover, when considering a large number of system states, misjudgments rarely occur, and their impact can be disregarded for reliability assessment. The validity of this assumption will also be discussed in Section IV.

D. Overall Process of the Proposed Method

The overall reliability assessment process of the proposed SS approach is shown in Fig. 3 and elaborated as follows:

Step 1: Input system data, annual curves, and preset parameters, including $N_{\max}$ (maximum iterations), *tol* (convergence accuracy), N_{MCS} (the number of sampled system states), and N_{T} (maximum contingency order).

Step 2: Create the system state set Ω_s by MCS or SE.

Step 3: Choose a system state $\boldsymbol{s}$ from Ω_s and construct the AC OPF model (2) - (10) accordingly.

Step 4: Choose a set of active constraints from Ω_a.

Step 5: Use the active constraints set to transform the AC OPF problem of state $\boldsymbol{s}$ into the state-similarity-based equations (23) - (25).

Step 6: Use the proposed alternating iterative approach to solve the equations.

Step 7: Evaluate the derived solution against the feasibility

criterion (43). If it satisfies the criterion, obtain the solution $\boldsymbol{X}^s$, and go to Step 8; otherwise, go to Step 9B.

Step 8: Evaluate the solution $\boldsymbol{X}^s$ against the optimality criteria (44) - (45). If it meets these criteria, go to Step 9A; otherwise, go to Step 9B.

Step 9A: The solution $\boldsymbol{X}^s$ is the optimal solution, and we can determine the optimal load curtailment.

Step 9B: Check if all active constraint sets in the state similarity set Ω_a have been used. If so, optimize the AC OPF problem to calculate the optimal load curtailment, incorporate its active constraints into Ω_a, and go to Step 9; otherwise, return to Step 4.

Step 10: Check if all $\boldsymbol{s}$ in the Ω_s have been evaluated. If so, go to Step 11; otherwise, go back to Step 3.

Step 11: Calculate reliability indices.

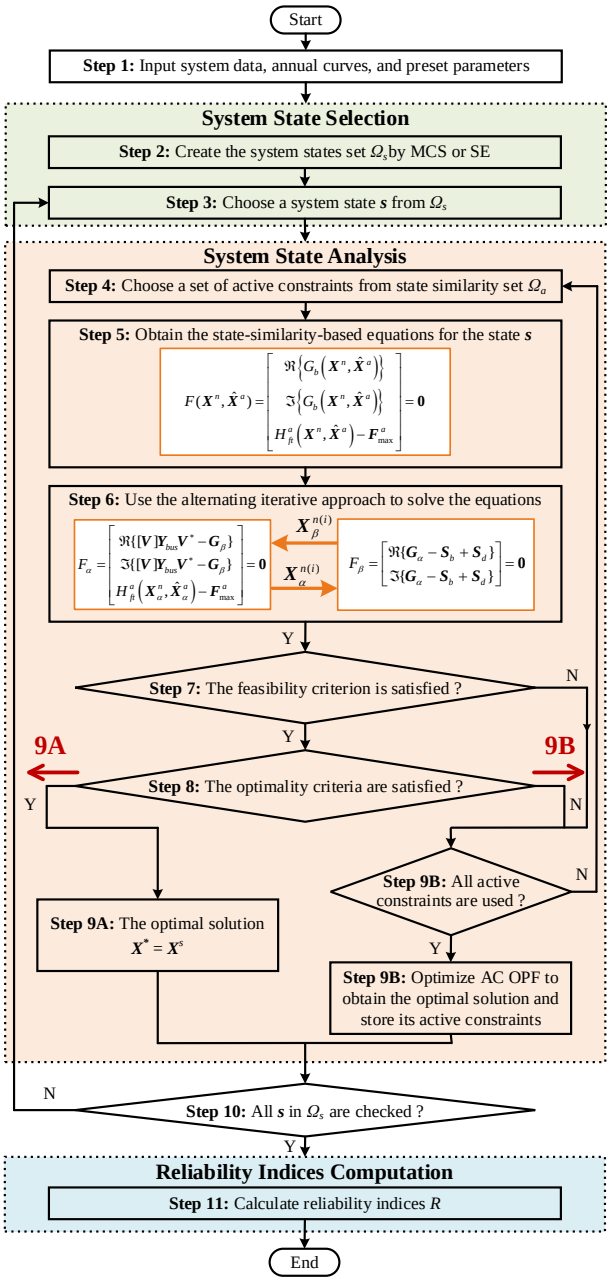

Fig. 3. The overall process of the proposed SS-based reliability assessment.

IV. Numerical Results

The proposed SS approach is utilized to assess the reliability of the RTS-79 [31], IEEE 118-bus [32], and Brazilian [33] systems. The performance of the SS approach is also investigated in power systems integrated with renewable energy. Annual load curves and renewable energy output curves are from Alberta [34] and NREL [35], [36], respectively. 100 load levels and REGs outputs are employed to characterize the fluctuations of loads and REGs. The unavailability data for branches and generators are presented in [21]. The IPOPT 3.12.9 is used as the optimization solver. The experiments are conducted using MATLAB® R2020b on a standard PC equipped with dual Intel® Xeon® Platinum 8180 CPU (ES) 28×1.8 GHz and 128 GB RAM.

A. Case I: Results on the RTS-79 System

RTS-79 system [31] is a composite power system with 24 buses, 33 generator units, and 38 branches. The total generation capacity is 3405 MW and the peak load is 2850 MW. The renewable generation penetration, denoted as ζ_{re}, is defined as the ratio of renewable generation to total generation capacity. The RTS-79 system is examined with specific levels of renewable generation penetration, which are 0%, 15%, and 30%. A specific portion of the capacity of each conventional generator is replaced with renewable energy sources. The ratio of this replacement is equal to the renewable generation penetration. Specifically, at each generator node, wind turbines and photovoltaics are integrated with a capacity ratio of 1:1. It is noted that when the penetration rate reaches 30%, the total generation capacity is expanded by 30% to accommodate this high level of renewable energy penetration and ensure system reliability.

The reliability assessment results of the SS approach combined with MCS, CEMCS, SE, and IISE methods (i.e., SSMCS, SSCEMCS, SSSE, and SSIISE methods) are used to show the excellent performance of the proposed SS method in Table V. The baseline of reliability results is determined by 1×10^8 sampled states. In general, this estimate can be regarded as the actual value, given the extensive number of samples involved. The preset parameters are given as follows: $N_{\max}$ = 10, *tol* = 0.1, N_T = 5, and β (the coefficient of variation for MCS) = 1%. The system states above third-order are only generation contingencies, which can cover 98.7778 % of system states for the SE method.

1) Efficiency and Accuracy

As shown in Table II, when ζ_{re} = 0%, the computation speed of the SS approach is approximately 20 times faster than that of the MCS, SE, and IISE methods. This is because only 1.54% of states in the MCS method and 3.21% of states in the SE or IISE method are analyzed by IPOPT independently. The optimal load curtailments of the remaining system states are solved by the state-similarity-based equations, which require minimal effort. Also, the approach error of SS is roughly 1%, which is generally considered negligible in the reliability assessment. This implies that the majority of the obtained solutions can be regarded as the optimal solutions to the

original AC OPF problems, given that most states follow the same active constraints. Consequently, state similarity emerges as a highly effective heuristic strategy for accelerating AC OPF computations.

Moreover, the CE-based sampling technique can significantly reduce the number of states, while it requires a complex pre-simulation to change the probability of system states and hasten the convergence. When coupled with the SS approach, the SSCEMCS method can achieve a substantial improvement in the efficiency of reliability assessment.

TABLE II
RELIABILITY ASSESSMENT RESULTS OF EIGHT METHODS (RTS-79)

ζ_{re} (%)	Method	EENS(MWh/y) Value	Relative Error* (%)	Approach Error† (%)	OPF Number‡	CPU Time(s)
0	Baseline	655.12	-	-	-	-
	MCS	662.68	1.15	-	24790000	40458
	SSMCS	669.39	2.18	1.01	381382	1396
	CEMCS	660.39	0.80	-	306000	543
	SSCEMCS	667.20	1.84	1.03	72102	160
	SE	395.57	39.62	-	24478200	36852
	SSSE	398.41	39.19	0.72	785244	2265
	IISE	605.66	7.55	-	24478200	36860
	SSIISE	609.64	6.94	0.66	785244	2272
15	Baseline	5757.06	-	-	-	-
	MCS	5760.52	0.06	-	3090000	5229
	SSMCS	5594.73	2.82	2.88	135540	362
	CEMCS	5729.04	0.49	-	121000	200
	SSCEMCS	5593.21	2.85	2.37	50751	109
	SE	4197.30	27.09	-	24478200	37168
	SSSE	4207.35	26.92	0.24	1300826	3715
	IISE	5132.34	10.85	-	24478200	37176
	SSIISE	5250.88	8.79	2.31	1300826	3724
30	Baseline	809.49	-	-	-	-
	MCS	815.32	0.72	-	20833000	40230
	SSMCS	807.47	0.25	0.96	361964	1502
	CEMCS	794.61	1.84	-	404000	758
	SSCEMCS	790.59	2.34	0.51	88565	211
	SE	536.40	33.74	-	24478200	49352
	SSSE	542.85	32.94	1.20	469721	1931
	IISE	769.06	4.99	-	24478200	49357
	SSIISE	774.44	4.33	0.70	469721	1938

*Relative Error is the difference between the results and the baseline.
†Approach Error is the difference in results when using methods with and without SS.
‡OPF number refers to the count of instances where optimization algorithms are employed to solve AC OPF problems.

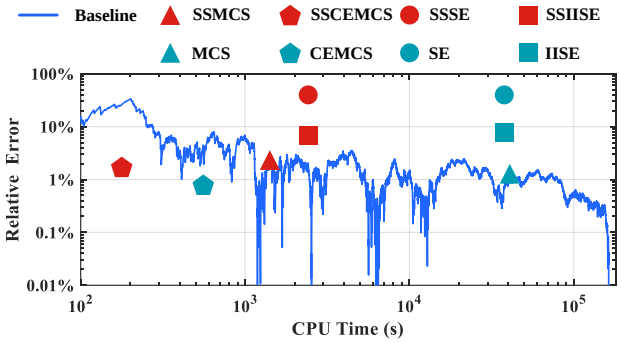

Fig. 4. Computational efficiencies of eight methods (RTS-79).

In addition, it is inappropriate to employ the SE method for the evaluation of larger systems due to the relative error in comparison to the baseline. To address this, the IISE method [9] has been developed to transfer the partial impacts of higher-order states to the corresponding lower-order ones. Therefore, the influence of the ignored higher-order ones is reduced, and the accuracy of IISE is significantly improved, as shown in Fig. 4. Notably, by integrating with the SS approach, SSIISE outperforms the conventional SE method in terms of both computing time and accuracy.

To illustrate the applicability of the proposed methods in systems with renewable energy, we conducted several cases with renewable generation penetrations of 5%, 15%, and 30%. As the ζ_{re} increases, a corresponding proportion of conventional generation capacity is replaced by renewable sources. Given the constant total generation capacity and load demand, the stochastic nature of renewable energy significantly reduces the system load supply capability. Consequently, with higher renewable penetrations, the power system reliability decreases, as indicated by the increase in reliability indices. Notably, when ζ_{re} reaches 30%, the increased generation capacity begins to counterbalance the supply uncertainty introduced by renewable energy, restoring the system reliability to levels nearly equivalent to those observed at ζ_{re} = 0%. Table II shows that the OPF number is larger than that of the system without renewable energy. This suggests that more state similarities (i.e., the set of active constraints) occur in the system due to intermittent renewable energy. Despite a slight decrease in accuracy and efficiency, the SS approach can still improve the computation speed at least 10 times. As a result, it can also achieve a preferable performance for the reliability assessment of power systems with renewable generators.

2) Verification of Accuracy Using One Load Curve Case

A single load curve for the RTS-79 system [31] is employed to validate the accuracy of the proposed reliability assessment methods. In this case, variable loads are represented by this load curve. Table III provides a comparative overview, illustrating that the reliability results from the SS methods align closely with those from the previous study [9]. The minor discrepancy can be attributed to the calculation error of the SS approach and the variance in MCS sampling. Moreover, as expected, the results from [37] and [38], which employ the DC OPF model, are lower than those calculated using the AC OPF model. Consequently, these comparisons demonstrate the reliable accuracy of the proposed SS methods.

TABLE III
RELIABILITY ASSESSMENT RESULTS OF ONE LOAD CURVE CASE (RTS-79)

Method	EENS(MWh/y) Value	Relative Error (%)	Approach Error (%)	OPF Number	CPU Time(s)
Baseline	1570.27	-	-	-	-
[9] AC OPF	1573.23	0.19	-	-	-
[37] DC OPF	1203.00	23.39	-	-	-
[38] DC OPF	1360.02	13.39	-	-	-
MCS	1589.02	1.19	-	12700000	19215
SSMCS	1595.53	1.61	0.41	249081	634
CEMCS	1592.61	1.42	-	496000	754
SSCEMCS	1595.43	1.60	0.18	91906	178
IISE	1302.57	17.05	-	24478200	36959
SSIISE	1303.45	16.99	0.07	143396	3348
SE	1576.30	0.38	-	24478200	36973
SSSE	1577.41	0.45	0.07	143396	3357

3) Impacts of Parameters N_{max} and tol

The convergence accuracy and speed of SS depend on the maximum iterations $N_{\max}$ and acceptable tolerance *tol*. Table IV presents the impact of these parameters on the SSIISE and SSCEMCS methods. When *tol* is reduced to 0.1 or lower, the error is about 1% or less. Additionally, when *tol* exceeds 0.001, all solutions obtained by SS closely approximate the optimal solutions. On the other hand, $N_{\max}$ has a slight impact on the precision, especially when $N_{\max} > 10$. It indicated that the proposed approach typically achieves desirable solutions within about 10 iterations for reliability assessment. If $N_{\max}$ is lower than 10, the iteratively obtained solutions often fail to meet the optimality criteria, making it challenging to achieve optimal solutions that could replace those derived from OPF computations. Therefore, as $N_{\max}$ increases, a great number of states can be evaluated by the state-similarity-based equations instead of OPF optimizations, thereby shortening the computational time. Additionally, when $N_{\max}$ exceeds 10, the computational time tends to stabilize. This indicates that the potential for further reducing the number of OPF calculations is nearly at its minimum and closely corresponds to the number of state similarity categories. Consequently, *tol* is set at 0.1 and $N_{\max}$ is available between 10 and 25 in this study.

TABLE IV
THE IMPACT OF N_{MAX} AND *TOL* ON RELIABILITY ASSESSMENT METHODS
(RTS-79 ζ_{re} = 0%)

Method	*tol*	$N_{\max}$	EENS(MWh/y)		OPF Number	CPU Time(s)
			Value	Approach Error (%)		
IISE	0.1	10	605.66	0	24478200	36860
SSIISE	0.5	5	805.78	33.04	744847	1788
		10	805.78	33.04	744847	1792
		20	805.78	33.04	744847	1803
	0.1	5	609.64	0.66	785416	2244
		10	609.64	0.66	785244	2272
		20	609.64	0.66	785225	2284
	0.01	5	606.68	0.16	3016681	6439
		10	606.99	0.22	787687	2968
		20	607.18	0.25	784796	2961
CEMCS	0.1	10	660.39	0	306000	543
SSCEMCS	0.5	5	864.55	30.92	61016	128
		10	864.55	30.92	61016	129
		20	864.55	30.92	61016	126
	0.1	5	667.20	1.03	72138	168
		10	667.20	1.03	72102	160
		20	667.20	1.03	72093	156
	0.01	5	661.46	0.16	96732	221
		10	661.59	0.18	71856	187
		20	661.68	0.20	71560	179

4) Analysis of Optimality Criteria

Since the active constraints between states may be different, the optimality criteria are crucial rules to ensure the accuracy of reliability assessment results. The minimal load curtailment of the new state is calculated through each set of active constraints from the state similarity set, and only the solutions that satisfy the optimality criteria are eligible for computing reliability indices.

The methods without optimality criteria may result in the acceptance of suboptimal solutions, potentially affecting the accuracy of reliability assessments. As shown in Table V, the optimality criteria have been utilized to correct 16779, 7154, and 41988 states for SSMCS, SSCEMCS, and SSIISE methods, respectively. These solutions that did not meet the criteria have been filtered out to enhance accuracy. Furthermore, Tables II and V also show that the optimality criteria can significantly enhance computational accuracy, albeit with a slight increase in computational time.

TABLE V
THE IMPACT OF OPTIMALITY CRITERIA ON THE PROPOSED SS METHODS
(RTS-79 ζ_{re} = 0%)

Method	EENS(MWh/y)		OPF Number	Optimality Criteria Correction	CPU Time(s)
	Value	Relative Error† (%)			
SSMCS	669.39	0	381382	16779	1396
SSMCS (-)*	1628.60	143.30	370971	-	1340
SSCEMCS	667.2	0	72102	7154	160
SSCEMCS (-)	1613.89	141.89	59903	-	122
SSIISE	609.64	0	785244	41988	2272
SSIISE (-)	1480.36	142.83	690554	-	2171

*(-) denotes methods without verifying the optimality criteria (44) and (45).
†**Relative Error** is the difference between methods with and without optimality criteria.

5) Reliability Assessment Results of PLC

Table VI presents the PLC results for the RTS-79 system with ζ_{re} values at 0% and 30%. Like the EENS results, the proposed SS methods can yield PLC values with low relative and approach errors, indicating their effectiveness in calculating PLC indices. Furthermore, the relative errors for PLC are usually lower than those for EENS. This is attributed to the faster convergence of PLC in MCS methods.

TABLE VI
RELIABILITY ASSESSMENT RESULTS OF PLC (RTS-79)

Method	ζ_{re} (%)	PLC ($\times 10^{-3}$)			ζ_{re} (%)	PLC ($\times 10^{-3}$)		
		Value	Relative Error (%)	Approach Error (%)		Value	Relative Error (%)	Approach Error (%)
Baseline	0	0.757	-	-	30	0.912	-	-
MCS		0.756	0.11	-		0.916	0.44	-
SSMCS		0.776	2.55	2.67		0.907	0.55	0.99
CEMCS		0.751	0.75	-		0.902	1.08	-
SSCEMCS		0.770	1.71	2.48		0.892	2.21	1.15
SE		0.505	33.21	-		0.661	27.52	-
SSSE		0.515	31.96	1.88		0.672	26.37	1.59
IISE		0.708	6.38	-		0.878	3.70	-
SSIISE		0.722	4.63	1.86		0.884	3.04	0.68

6) Examples of State-Similarity-based Solving Process

To analyze the iterative solution process of the SS approach, the following three states are considered. The contingency scenario and active constraints of the base state are shown in Fig. 5. In this case, bus 3 becomes a terminal bus due to the failure of branches 3-24 and 3-1. The active constraints exhibit a pattern that aims to minimize load curtailment through several strategies: shedding the load at Bus 3, elevating the voltages of several buses to their upper limits, and operating branch 3-9 at maximum capacity. The maximum power supply of bus 3 is primarily constrained by transmission capacity, with load variations having a marginal impact. Therefore, this pattern can be regarded as a physical representation of state similarity. In the following states, the state 1 (S1) exhibits state similarity with the base state, while the state 2 (S2) does not. The solutions of these two states through the SS approach are presented in Table VII.

The base state and S1 have the same active constraints, and

the solution to S1 can be regarded as the optimal solution with acceptable error. Fig. 6 shows the iterative process of S1 using SS and IP. The SS approach seeks the solution in the vicinity of the optimum, with the solution from the first iteration being very close to the optimal values. In contrast, the IP method iterates toward an optimal solution along the interior of the feasible region, initially moving away and then rapidly converging to the optimum. Both the SS and IP solutions satisfy the optimality criteria within an acceptable margin of numerical error.

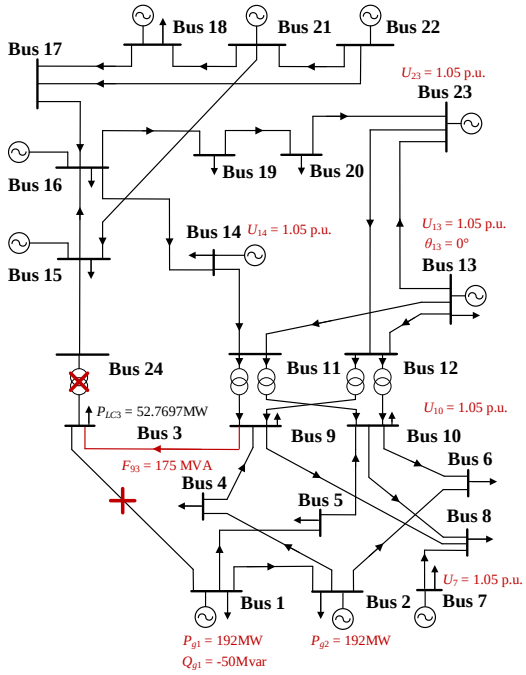

Fig. 5. AC OPF results for RTS-79 system with branch failures 1-3 and 3-24. The active constraints of the base state are highlighted in red.

TABLE VII
THE RESULTS OF SS AND IP FOR TWO EXAMPLES

State	Bus 3 Load (MW)	System Load (MW)	Methods	Load Curtailment of Bus 3 (MW)	Iterations Number	Optimality Criteria
Base	216	2445	IP*	52.7697	21	-
S1	169	2292	IP	5.7547	16	-
			SS	5.7539	4	true
S2	163	2068	IP	0	22	-
			SS	0.0682	2	false

*IP is the Interior Point method implemented by the IPOPT solver. The solution of the base state is used as the original variables to solve the AC OPF problems of S1 and S2.

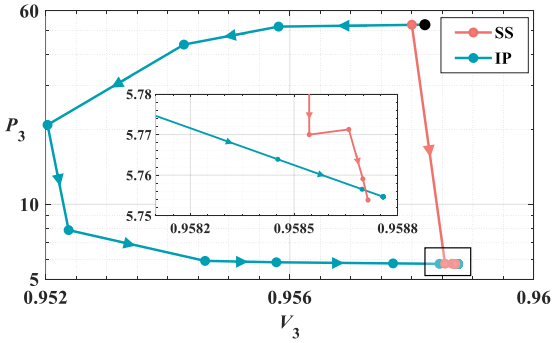

Fig. 6. The iteration process of S1.

In S2, the results with no load curtailment suggest that the active constraints in S2 differ from those in the base state. As shown in Table VII, the SS solution, derived from the active constraints of the base state, is a suboptimal solution to the AC OPF problem. Since the optimality criteria (44) and (45) are not satisfied, there is no state similarity between S2 and the base state. Therefore, this SS solution should be rejected. Subsequently, S2 will be resolved using other active constraints. If S2 fails to match any set of active constraints, its accurate solution must be analyzed using the IP method.

TABLE VIII
RELIABILITY ASSESSMENT RESULTS OF EIGHT METHODS (IEEE 118-BUS)

ζ_{re} (%)	Method	EENS(MWh/y) Value	Relative Error (%)	Approach Error (%)	OPF Number	CPU Time(s)
0	Baseline	261.40	-	-	-	-
	MCS	260.96	0.17	-	13240000	52547
	SSMCS	265.06	1.40	1.57	403533	2107
	CEMCS	262.67	0.49	-	1490000	5771
	SSCEMCS	264.93	1.35	0.86	489725	2403
	SE	157.62	39.70	-	2892100	8709
	SSSE	159.61	38.94	1.27	64866	609
	IISE	239.99	8.19	-	2892100	8710
	SSIISE	244.12	6.61	1.72	64866	609
15	Baseline	458.21	-	-	-	-
	MCS	464.95	1.47	-	8550000	31851
	SSMCS	459.09	0.19	1.26	329566	1490
	CEMCS	455.86	0.51	-	636000	2671
	SSCEMCS	450.46	1.69	1.18	244131	1132
	SE	247.20	46.05	-	2892100	8856
	SSSE	251.33	45.15	1.67	74834	845
	IISE	417.88	8.80	-	2892100	8856
	SSIISE	418.52	8.66	0.15	74834	846
30	Baseline	268.29	-		-	-
	MCS	267.58	0.27	-	13290000	46804
	SSMCS	266.86	0.53	0.27	428185	2147
	CEMCS	269.89	0.60	-	1510000	6247
	SSCEMCS	266.86	0.53	1.12	445727	2066
	SE	158.95	40.75	-	2892100	8918
	SSSE	161.00	39.99	1.28	103550	678
	IISE	237.86	11.34	-	2892100	8919
	SSIISE	234.66	12.53	1.34	103550	678

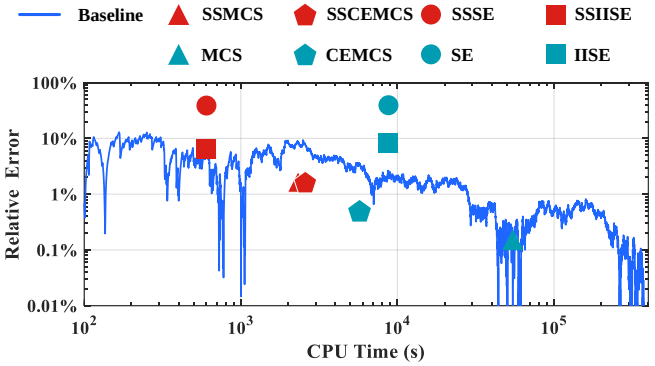

Fig. 7. Computational efficiencies of six methods (IEEE-118).

B. Case II: Results on the IEEE 118-Bus System

IEEE 118-bus system [32] consists of 118 buses, 54 generation units, and 186 branches. The total generation capacity is 99 662 MW and the peak load is 42 420 MW. The maximum contingency order for SE is 2, and the other parameters are the same as those in Case I.

1) Accuracy and Efficiency

As shown in Table VIII, the computation speed of MCS and

SE can be accelerated over 10 times by utilizing the SS approach within the IEEE 118-bus system. Fig. 7 demonstrates that both SSMCS and SSCEMCS display superior computational speed and accuracy, while CEMCS holds a relatively high level of computational precision. The proposed SS approach can yield relatively accurate results, with an error margin of approximately 2% for MCS and less than 10% for SE. CEMCS serves as a beneficial method for enhancing MCS efficiency, which can be further improved by the SS approach. Consequently, the proposed SS approach has the potential to improve the efficiency of reliability assessment for the IEEE 118-bus system. Similar to Case I, the increasing renewable energy results in the reliability degradation for the IEEE 118-bus system.

2) Analysis of optimality criteria

Table IX shows the reliability assessment results from the proposed SS methods with and without optimality criteria. These criteria can be used to match the state with the appropriate active constraints, thereby ensuring the precision of reliability evaluation. Compared with MCS methods, states up to the second order in SSIISE more efficiently align with active constraints, resulting in fewer corrective actions by the optimality criteria. Consequently, the proposed method with optimality criteria can significantly enhance the overall computational efficiency of reliability assessment.

TABLE IX
THE IMPACT OF OPTIMALITY CRITERIA ON THE PROPOSED SS METHODS (IEEE 118-BUS ζ_{re} = 0%)

Method	EENS(MWh/y)		OPF Number	Optimality Criteria Correction	CPU Time(s)
	Value	Relative Error† (%)			
SSMCS	265.06	0	403533	4241	2107
SSMCS (-)*	650.33	145.35	396559	-	1944
SSCEMCS	264.93	0	489725	19438	2403
SSCEMCS (-)	597.55	125.55	450368	-	2011
SSIISE	244.12	0	64866	43	609
SSIISE (-)	293.09	20.06	64669	-	473

C. Case III: Results on the Brazilian System

Brazilian system [33], an equivalent network of the southern region of Brazil, consists of 242 buses, 52 generation units, and 489 branches. The total generation capacity is 206 023 MW and the peak load is 185 276 MW. The results of 2×10^8 sampled states are used as the baselines with ζ_{re} at 0% and 30%, and N_T = 3. The other parameters are consistent with those in Case I, and the reliability results of the Brazilian system are listed in Table X.

The SSMCS and SSCEMCS methods demonstrate significant efficiency in reducing computational time while maintaining high accuracy. For instance, at ζ_{re} = 0%, the computational time for SSMCS is approximately 25 times faster than that of the MCS method, with only a minimal approach error for EENS. Compared to traditional SE methods, the proposed SS method significantly reduces computation time by over 10 times. However, the SE and IISE methods exhibit considerable deviations in EENS values compared to the baseline. This indicates that these methods may not be sufficiently accurate for assessing system reliability in complex systems like the Brazilian system, likely due to their inability to analyze higher-order states. Table X also shows a wide variety of state similarities, attributed to the numerous topological changes caused by component failures. Future improvements will focus on enhancing the applicability to identify state similarities across different component failure states.

TABLE X
RELIABILITY ASSESSMENT RESULTS OF EIGHT METHODS (BRAZILIAN)

ζ_{re} (%)	Method	EENS(MWh/y)			OPF Number	CPU Time(s)
		Value	Relative Error (%)	Approach Error (%)		
0	Baseline	170.05	-	-	-	-
	MCS	169.77	0.21	-	186300000	1165106
	SSMCS	169.56	0.33	0.13	7317665	50564
	CEMCS	166.64	2.05	-	18830000	120988
	SSCEMCS	166.99	1.84	0.21	3828739	35642
	SE	15.37	90.96	-	14225500	87984
	SSSE	15.54	90.87	1.05	655734	6683
	IISE	93.07	45.29	-	14225500	87989
	SSIISE	94.01	44.74	1.01	655734	6685
30	Baseline	169.97	-	-	-	-
	MCS	170.26	0.17	-	178600000	1141798
	SSMCS	171.04	0.63	0.45	7666968	54116
	CEMCS	165.11	2.86	-	19210000	122435
	SSCEMCS	164.49	3.22	0.37	3843582	34635
	SE	16.61	90.23	-	14225500	91107
	SSSE	16.49	90.30	0.72	552563	5120
	IISE	100.51	40.86	-	14225500	91112
	SSIISE	99.79	41.29	0.72	552563	5122

V. CONCLUSION

This paper proposes a state-similarity-based approach to accelerate the reliability assessment of power systems considering variations in renewable generation and loads. As empirical evidence and experience show, multiple states often share similar active constraints with only minor differences in generator outputs and load levels. Based on this state similarity, the AC OPF computations can be streamlined to solving nonlinear equations. Furthermore, an alternating iterative approach is proposed to get an approximate solution to these equations, which can effectively obtain the minimal load curtailment of the original AC OPF problem. The optimality criteria are implemented to match states with their similarities and to reject the vast majority of inaccurate solutions. The results demonstrate that the proposed method can remarkably speed up the reliability assessment. More than 90% of states are analyzed by the SS approach instead of time-consuming optimization algorithms. Its effectiveness is also proven in renewable energy systems, in some cases improving speed by more than 10 times with high accuracy. Moreover, the robustness and applicability of the proposed SS approach are demonstrated in various systems, from the RTS-79 to the Brazilian system, indicating its suitability for complex power systems.

REFERENCES

[1] R. Billinton and W. Li, *Reliability Assessment of Electrical Power Systems Using Monte Carlo Methods*. New York, NY, USA: Springer, 1994.

[2] W. Li, *Risk Assessment of Power Systems: Models Methods and Applications*. Hoboken, NJ, USA: Wiley, 2014.

[3] C. Singh and J. Mitra, "Composite System Reliability Evaluation Using State Space Pruning," *IEEE Trans. Power Syst.*, vol. 12, no. 1, pp. 471-479, 1997.

[4] J. L. Cai, L. L. Hao, Q. S. Xu, and K. Q. Zhang, "Reliability Assessment of Renewable Energy Integrated Power Systems with an Extendable Latin Hypercube Importance Sampling Method," *Sustain. Energy Techn.*, vol. 50, Mar. 2022.

[5] Y. Zhao, Y. Sun, H. Ren, K. Xie, W. Li, and J. Yu, "Probability Density Estimation for Composite Systems Reliability Indices Using Cross-Entropy Based Continuous Time Markov Chain Simulation," *IEEE Trans. Power Syst.*, vol. 39, no. 2, pp. 2749-2762, March 2024.

[6] Y. Ding, P. Wang, L. Goel, P. C. Loh, and Q. Wu, "Long-Term Reserve Expansion of Power Systems with High Wind Power Penetration Using Universal Generating Function Methods," *IEEE Trans. Power Syst.*, vol. 26, no. 2, pp. 766-774, May 2011.

[7] A. M. Rei and M. T. Schilling, "Reliability Assessment of the Brazilian Power System Using Enumeration and Monte Carlo," *IEEE Trans. Power Syst.*, vol. 23, no. 3, pp. 1480-1487, Aug. 2008.

[8] Y. Jia, P. Wang, X. Han, J. Tian, and C. Singh, "A Fast Contingency Screening Technique for Generation System Reliability Evaluation," *IEEE Trans. Power Syst.*, vol. 28, no. 4, pp. 4127-4133, Nov. 2013.

[9] K. Hou, H. Jia, X. Li, X. Xu, Y. Mu, T. Jiang, and X. Yu, "Impact-increment Based Decoupled Reliability Assessment Approach for Composite Generation and Transmission Systems," *IET Gener. Transm. Distrib.*, vol. 12, no. 3, pp. 586-595, Feb. 2018.

[10] Y. K. Lei et al., "Impact Increment Based Hybrid Reliability Assessment Method for Transmission Systems," *CSEE J. Power Energy*, vol. 8, no. 1, pp. 317-328, Jan. 2022.

[11] Hua Wei, H. Sasaki, J. Kubokawa, and R. Yokoyama, "An Interior Point Nonlinear Programming for Optimal Power Flow Problems with A Novel Data Structure," in *Proc. 20th Int. Conf. Power Ind. Comput. Appl.*, 1997, pp. 134-141.

[12] Q. Li and V. Vittal, "Non-Iterative Enhanced SDP Relaxations for Optimal Scheduling of Distributed Energy Storage in Distribution Systems," *IEEE Trans. Power Syst.*, vol. 32, no. 3, pp. 1721-1732, May 2017.

[13] Y. J. Jia, X. Q. Bai, L. Q. Zheng, Z. L. Weng, and Y. Y. Li, "ConvOPF-DOP: A Data-Driven Method for Solving AC-OPF Based on CNN Considering Different Operation Patterns," *IEEE Trans. Power Syst.*, vol. 38, no. 1, pp. 853-860, Jan. 2023.

[14] M. Zhou, M. H. Chen, and S. H. Low, "DeepOPF-FT: One Deep Neural Network for Multiple AC-OPF Problems with Flexible Topology," *IEEE Trans. Power Syst.*, vol. 38, no. 1, pp. 964-967, Jan. 2023.

[15] S. Chatzivasileiadis, A. Venzke, J. Stiasny, and G. Misyris, "Machine Learning in Power Systems: Is It Time to Trust It?" *IEEE Power Energy M.*, vol. 20, no. 3, pp. 32-41, May-Jun. 2022.

[16] L. Zhang, Y. Z. Chen, and B. S. Zhan, "A Convex Neural Network Solver to DCOPF With Generalization Guarantees," *IEEE Trans. Control Netw.*, vol. 9, no. 2, pp. 719-730, Jun. 2022.

[17] A. Safdarian, M. Fotuhi-Firuzabad, F. Aminifar, and M. J. Ghorbany, "Composite Power System Adequacy Assessment Based on the Post Optimal Analysis," *Turk. J. Elec. Eng. Comput. Sci.*, vol. 21, no. 1, pp. 90-106, Jan. 2013.

[18] P. Yong, N. Zhang, C. Kang, Q. Xia, and D. Lu, "MPLP-based Fast Power System Reliability Evaluation Using Transmission Line Status Dictionary," *IEEE Trans. Power Syst.*, vol. 34, no. 2, pp. 1630-1640, Mar. 2019.

[19] Z. Zhuo, E. Du, N. Zhang, C. Kang, Q. Xia, and Z. Wang, "Incorporating Massive Scenarios in Transmission Expansion Planning with High Renewable Energy Penetration," *IEEE Trans. Power Syst.*, vol. 35, no. 2, pp. 1061-1074, Mar. 2020.

[20] D. Deka and S. Misra, "Learning for DC-OPF: Classifying active sets using neural nets," in *Proc. IEEE Milan PowerTech*, 2019, pp. 1-6.

[21] Z. Liu, K. Hou, H. Jia, J. Zhao, D. Wang, Y. Mu, and L. Zhu, "A Lagrange Multiplier Based State Enumeration Reliability Assessment for Power Systems with Multiple Types of Loads and Renewable Generations," *IEEE Trans. Power Syst.*, vol. 36, no. 4, pp. 3260-3270, Jul. 2021.

[22] Z. Liu, P. Tang, K. Hou, L. Zhu, J. Zhao, H. Jia, W. Pei, "A Lagrange-multiplier-based Reliability Assessment for Power Systems Considering Topology and Injection Uncertainties," *IEEE Trans. Power Syst.*, vol. 39, no. 1, pp. 1178-1189, Jan 2024.

[23] D. G. Luenberger, *Linear and Nonlinear Programming*. New York, NY, USA: Springer, 2005.

[24] F. Hasan, A. Kargarian and A. Mohammadi, "A Survey on Applications of Machine Learning for Optimal Power Flow," in *Proc. IEEE Texas Power Energy Con.*, 2020, pp. 1-6.

[25] F. Hasan, A. Kargarian, and J. Mohammadi, "Hybrid Learning Aided Inactive Constraints Filtering Algorithm to Enhance AC OPF Solution Time," *IEEE Trans. Ind. Appl.*, vol. 57, no. 2, pp. 1325-1334, Mar.-Apr. 2021.

[26] Lloyd N. Trefethen and David Bau, *Numerical Linear Algebra*. Philadelphia, Pennsylvania, USA: SIAM, 1997.

[27] S. J. Leon, *Linear Algebra with Applications*, NJ, Englewood Cliffs: Prentice-Hall, 1994.

[28] J. Lavaei and S. H. Low, "Zero Duality Gap in Optimal Power Flow Problem," *IEEE Trans. Power Syst.*, vol. 27, no. 1, pp. 92-107, Feb. 2012.

[29] H. W. Dommel and W. F. Tinney, "Optimal Power Flow Solutions," *IEEE Trans. Power Appar. Syst.*, vol. PAS-87, no. 10, pp. 1866-1876, Oct. 1968.

[30] X. Tong, F. F. Wu, Y. Zhang, Z. Yan, and Y. Ni, "A Semismooth Newton Method for Solving Optimal Power Flow," *J. Ind. Manag. Optim.*, vol. 3, no. 3, pp. 553-567, Aug. 2007.

[31] P. M. Subcommittee, "IEEE Reliability Test System," *IEEE Trans. Power App. Syst.*, vol. PAS-98, no. 6, pp. 2047-2054, Nov. 1979.

[32] *IEEE 118-bus system*, Illinois Center for a Smarter Electric Grid, Information Trust Institute, University of Illinois, Oct. 2013. [Online]. Available: https://icseg.iti.illinois.edu/ieee-118-bus-system/

[33] Brazilian system reliability data, Github, Aug. 2021. [Online]. Available: https://github.com/ProfFernandoAssis/ReliabilityData.

[34] *Hourly load data by area and region from January 1, 2011 to December 31, 2016*, Alberta Electric System Operator (AESO), Apr. 2018. [Online]. Available: https://www.aeso.ca/market/market-and-system-reporting/data-requests/hourly-load-by-area-and-region/

[35] *Solar power data for integration studies*, National Renewable Energy Laboratory (NREL), 2007. [Online]. Available: https://www.nrel.gov/grid/solar-power-data.html

[36] *Eastern and western wind integration data sets*, National Renewable Energy Laboratory (NREL), 2014. [Online]. Available: https://www.nrel.gov/grid/eastern-western-wind-data.html

[37] Y. Zhao, Y. Tang, W. Y. Li, and J. Yu, "Composite Power System Reliability Evaluation Based on Enhanced Sequential Cross-Entropy Monte Carlo Simulation," *IEEE Trans. Power Syst.*, vol. 34, no. 5, pp. 3891-3901, Sep. 2019.

[38] R. Billinton and W. Y. Li, "Composite System Reliability Assessment Using a Monte-Carlo Approach," *IEE Conf. Publ.*, vol. 338, pp. 53-57, 1991.

Zeyu Liu received the B.S. degree from Tianjin University, Tianjin, China, in 2018. He is currently working toward the Ph.D. degree in the School of Electrical and Information Engineering, Tianjin University.

His research interests include power system reliability assessment, uncertainty analysis, and integrated energy systems planning and reliability evaluation.

Lewei Zhu (M'16) received the Ph.D. degree in Electrical Engineering from Tianjin University, Tianjin, China, in 2019.

She is currently a Lecturer at Maritime College in Tianjin University of Technology, Tianjin, China. Her research interests include dielectric failure mechanisms of cable insulation materials, power equipment insulation aging, and risk assessments of power systems.

Kai Hou (M'16, SM' 24) received the Ph.D. degree in Electrical Engineering from Tianjin University, Tianjin, China, in 2016.

He is currently an Associate Professor with Tianjin University. His research interests include reliability and resilience assessments of power systems, smart grids, and integrated energy systems.

Yue Zhou (M'16) received the Ph.D. degree in Electrical Engineering from Tianjin University, Tianjin, China, in 2016.

He is currently a Lecturer in cyber–physical systems with the School of Engineering, Cardiff University, Cardiff, U.K. His research interests include demand response, peer-to-peer energy trading, and cyber–physical systems.

Ruifeng Zhao (M'13) received the Ph.D. degree from Chongqing University, Chongqing, China in 2013.

He is currently a Senior Engineer with the Electric Power Dispatching and Control Center, Guangdong Power Grid Company Ltd., Guangdong, China. His research interests include automatic generation control, operation and control and optimization techniques in power systems and software engineering, information system development, and integration of power systems.

Hongjie Jia (M'04, SM'17) received the B.S., M.S., and Ph.D. degrees in Electrical Engineering from Tianjin University, Tianjin, China, in 1996, 1999, and 2001, respectively.

He is currently a Professor with Tianjin University. His research interests include power system reliability assessment, stability analysis and control, distribution network planning and automation, smart grids, and integrated energy systems.